(ニコランジル)，Trapidil(トラピジル)，Urapidil(ウラピジル)およびBisacodyl(ビサコジル)，Trihexyphenidyl(トリヘキシフェニジル)の塩酸塩が日局に収載されている。また，Bepridil(ベプリジル)の塩酸塩，Minoxidil(ミノキシジル)，Naftopidil(ナフトピジル)も日本で承認されている(図２)。

プロスタグランジンE_1(PGE_1)であるアルプロスタジルは，エイコサノイドの１つである。アルプロスタジルは，血管平滑筋弛緩作用を有し血流量を増加させ，さらに血小板凝集抑制作用を示す。慢性動脈閉塞症における四肢潰瘍ならびに安静時疼痛の改善，振動病における末梢血行障害に伴う自覚症状の改善ならびに末梢循環・神経・運動機能障害の回復，血行再建術後の血流維持などに適応される。

イフェンプロジルの酒石酸塩は，血管平滑筋直接弛緩作用や交感神経α受容体遮断作用により脳動脈血流量を増加させ，脳内のブドウ糖，ATP，乳酸などの代謝を改善することから，脳循環・代謝改善薬に分類され，脳梗塞後遺症，脳出血後遺症に伴うめまいの改善などに適応される。

ニコランジルは，ATP依存性カリウムチャネル開口薬であり，この作用によって血管平滑筋の拡張を引き起こすとともに，ニトロ基から内因性血管拡張物質であるNOが発生することにより末梢血管拡張作用が発現する。冠血管拡張作用があり，狭心症治療薬として使用される。

トラピジルは，トロンボキサンA合成酵素を阻害し冠血管拡張作用や抗血小板作用を示し，狭心症薬として使用される。

ウラピジルは，交感神経抑制性降圧薬の１つであり，アドレナリンα_1遮断作用を有する。高血圧治療あるいは排尿障害改善に用いられる。

ビサコジルは，フェノールエステル系大腸刺激薬で下剤として用いられる。

トリヘキシフェニジルの塩酸塩は，ビペリジン系の中枢性コリン作用薬であり，向精神薬投与によるパーキンソニズム・ジスキネジア・アカシジアおよび特発性パーキンソニズムおよびその他のパーキンソニズムに効能・効果を有する。

ベプリジルの塩酸塩は，細胞のカルシウムチャネルを抑制し，冠血管を拡げ心拍数を減少させる。不整脈・狭心症治療に用いられる。

ミノキシジルは，最初，高血圧の経口薬として開発された。その後，髪を育成し脱毛症を回復させる効果が発見された。日本では，医療用の実績がないまま一般用医薬品として承認されたダイレクトOTC第１号である。

ナフトピジルは，アドレナリンα_1受容体遮断薬であり，排尿困難治療に用いられる。

ステム「-dilol」を持つ血管拡張薬としては，Carvedilol(カルベジロール)，Nipradilol(ニプラジロール)が，ステム「-pendyl」を持つ血管拡張薬としては，Isothipendyl(イソチペンジル)の塩酸塩が日本で使われている(図３)。

カルベジロールは，アドレナリン$\alpha_1\beta$受容体に対する非選択的遮断薬であり，本態性高血圧症や狭心症の治療に用いられる。

ニプラジロールは，アドレナリンβ_1受容体非選択的な遮断薬であり，本態性高血圧治療，狭心症，緑内障高眼圧症治療に用いられる。

イソチペンジルの塩酸塩は，抗ヒスタミン作用，抗アレルギー作用を有する一般用薬として販売されている。

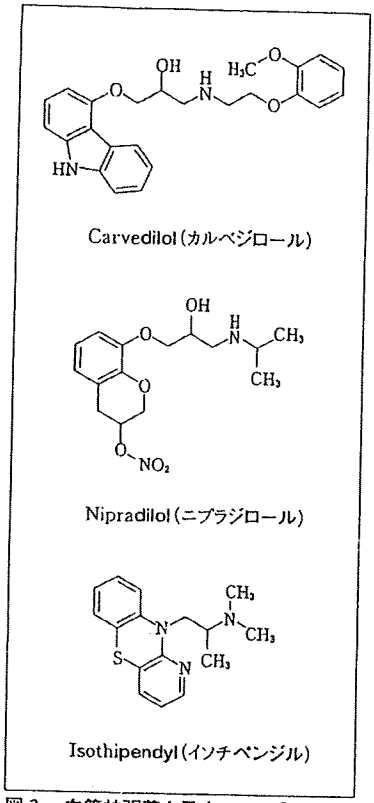

図3　血管拡張薬を示すステム「-dilol」，「-pendyl」を持つ医薬品

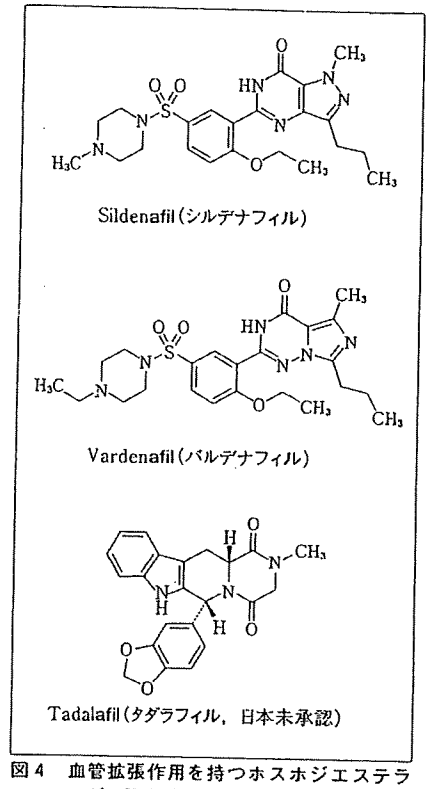

図4　血管拡張作用を持つホスホジエステラーゼ5阻害薬を示すステム「-afil」を持つ医薬品

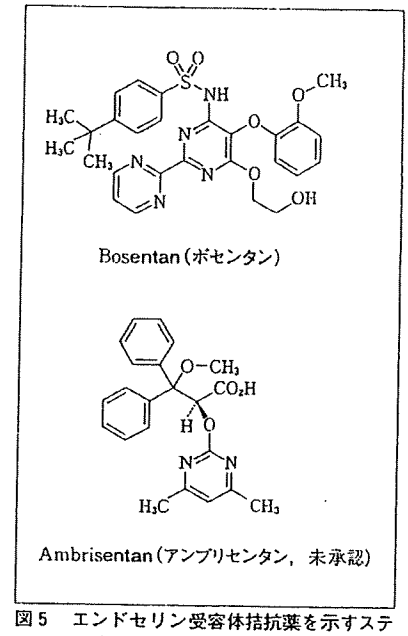

図5　エンドセリン受容体拮抗薬を示すステム「-entan」を持つ医薬品

「-afil」：血管拡張作用を持つホスホジエステラーゼ5阻害薬

「-afil」は，血管拡張作用を持つ5型ホスホジエステラーゼ阻害薬を示すステムである。5型ホスホジエステラーゼ（PDE5）はcGMPを分解する酵素であり，PDE5が阻害されると細胞内のcGMPが増加する。cGMPの増加は，内因性の血管拡張因子であるNOによる作用と同じであり，NO作動性神経に作用して血管を拡張させる。

ステム「-afil」を持ち日本で使用されている医薬品としては，Sildenafil（シルデナフィル），Vardenafil（バルデナフィル）が，また日本では未承認であるがTadalafil（タダラフィル）がある（図4）。シルデナフィルのクエン酸塩およびバルデナフィルの塩酸塩は，勃起不全治療薬として認可されている。米国で認可されているタダラフィルも勃起不全治療に用いられている。

「-entan」：エンドセリン受容体拮抗薬

「-entan」は，エンドセリン受容体拮抗薬を示すステムである。エンドセリンは，血管内皮細胞から分泌される21個のアミノ酸で構成されるペプチドであり，血管系や心筋組織に存在するエンドセリン受容体に作用して血管を収縮させる。エンドセリン受容体に拮抗作用する薬物は高血圧治療薬として開発されている。日本では，2005年にBosentan（ボセンタン）の水和物が肺動脈性肺高血圧症治療薬として承認されており，Ambrisentan（アンブリセンタン）も肺動脈性肺高血圧症薬として承認申請中である（図5）。

以上，今回は，平滑筋に作用する医薬品のステムとして，「-verine」，「-dil」，「-dyl」，「-dilol」，「-pendyl」，「-afil」，「-entan」を紹介した。

■参考文献
本稿作成に際して，前回までに紹介した参考文献を使用した。

Wide-Ranging Molecular Mobilities of Water in Active Pharmaceutical Ingredient (API) Hydrates as Determined by NMR Relaxation Times

SUMIE YOSHIOKA, YUKIO ASO, TSUTOMU OSAKO, TORU KAWANISHI

National Institute of Health Sciences, 1-18-1 Kamiyoga, Setagaya-ku, Tokyo 158-8501, Japan

Received 10 October 2007; revised 27 November 2007; accepted 28 November 2007

Published online 6 February 2008 in Wiley InterScience (www.interscience.wiley.com). DOI 10.1002/jps.21294

ABSTRACT: In order to examine the possibility of determining the molecular mobility of hydration water in active pharmaceutical ingredient (API) hydrates by NMR relaxation measurement, spin–spin relaxation and spin–lattice relaxation were measured for the 11 API hydrates listed in the Japanese Pharmacopeia using pulsed ^{1}H-NMR. For hydration water that has relatively high mobility and shows Lorentzian decay, molecular mobility as determined by spin–spin relaxation time (T_2) was correlated with ease of evaporation under both nonisothermal and isothermal conditions, as determined by DSC and water vapor sorption isotherm analysis, respectively. Thus, T_2 may be considered a useful parameter which indicates the molecular mobility of hydration water. In contrast, for hydration water that has low mobility and shows Gaussian decay, T_2 was found not to correlate with ease of evaporation under nonisothermal conditions, which suggests that in this case, the molecular mobility of hydration water was too low to be determined by T_2. A wide range of water mobilities was found among API hydrates, from low mobility that could not be evaluated by NMR relaxation time, such as that of the water molecules in pipemidic acid hydrate, to high mobility that could be evaluated by this method, such as that of the water molecules in ceftazidime hydrate.
 J Pharm Sci 97:4258–4268, 2008
Keywords: NMR relaxation time; dynamics; hydrate; DSC; water vapor sorption isotherm

INTRODUCTION

Correlations between chemical stability and molecular mobility have been demonstrated for various amorphous pharmaceuticals in the solid state.[1] Furthermore, the chemical stability of active pharmaceutical ingredient (API) hydrates is suggested to be correlated with the molecular mobility of water of hydration present in the crystalline structure.[2,3]

Water molecules in API hydrates exhibit a variety of physical states,[4,5] suggesting a range of molecular mobilities; water molecules incorporated into rigid crystalline structures may have low molecular mobility, whereas less rigid structures contain water molecules with greater mobility. Hydration water plays an important role in determining the physical characteristics—such as solubility[6] and flowability—of the API hydrate. Therefore, an understanding of the physical properties of hydration water, such as molecular mobility, is critical in the formulation of API hydrates.

The molecular mobility of water in solids may be determined by various methods, such as dielectric relaxation spectroscopy[7] and FT-Raman

Correspondence to: Sumie Yoshioka (Telephone: 81-3-3700-8547; Fax: 81-3-3707-6950; E-mail: yoshioka@nihs.go.jp)

Journal of Pharmaceutical Sciences, Vol. 97, 4258–4268 (2008)

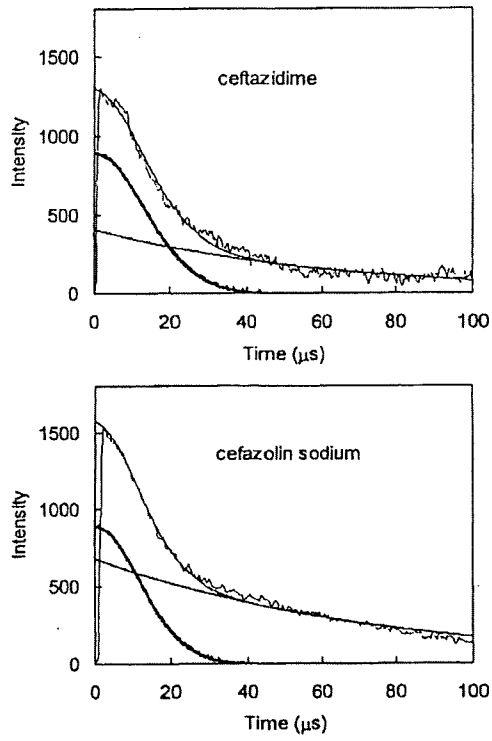

Figure 1. Free induction decay for ceftazidime and cefazolin sodium hydrates.

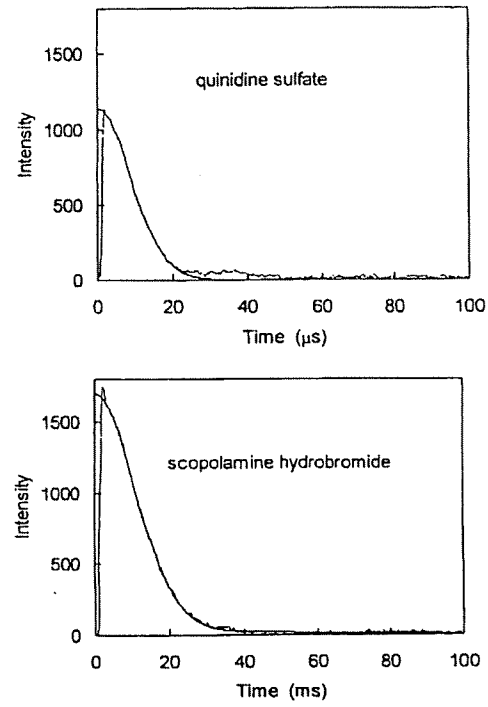

Figure 2. Free induction decay for quinidine sulfate and scopolamine hydrobromide hydrates.

spectroscopy.[8] NMR is also utilized to determine the molecular mobility of water in the solid state,[9] and to examine the various mechanisms by which solids interact with water.[10,11] However, there have been few studies in which the molecular mobility of water in API hydrates was determined using NMR. This may be because ^{1}H-NMR, even high resolution ^{1}H-NMR, cannot separate the peaks of the water protons from those of the protons in other components, which prevents specific determination of water mobility. Although the preparation of API hydrate samples using ^{17}O-labeled water allows to specifically determine the mobility of the water molecules by ^{17}O-NMR, unaffected by the other components, this approach requires high cost and much labor.

Table 1. Water Content of API Hydrates

API Hydrate	Number of H_2O per Molecule Specified in JP	Number of H_2O per Molecule Determined by KF	Spin–Spin Relaxation of H_2O
Cefazolin sodium	5	4.67	Lorentzian
Ceftazidime	5	5.04	Lorentzian
Amoxicillin	3	2.94	Lorentzian
Ampicillin	3	2.96	Lorentzian
Berberine Chloride	Not specified	2.67	Gaussian
Quinine hydrochloride	2	1.31	Gaussian
Scopolamine hydrobromide	3	2.32	Gaussian
Saccharin sodium	2	1.15	Gaussian
Pipemidic acid	3	2.9	Gaussian
Sulpyrine	1	0.98	Gaussian
Quinidine sulfate	2	1.95	Gaussian

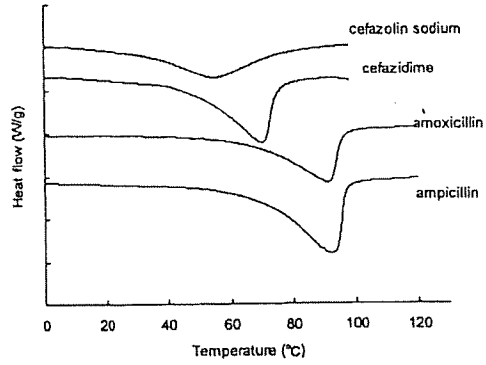

Figure 3. DSC thermograms for four antibiotic hydrates.

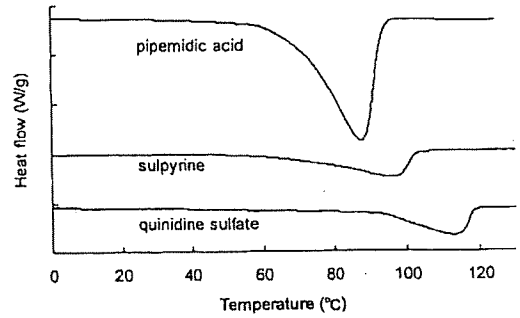

Figure 5. DSC thermograms for API hydrates showing a single endothermic peak.

Thus, determination of the molecular mobility of hydration water in API hydrates using NMR holds some challenges.

However, it is possible to determine the molecular mobility of hydration water in API hydrates by spin–spin relaxation measurement, if the spin–spin relaxation time (T_2) of the water protons is significantly different from that of the API protons. Furthermore, the spin–lattice relaxation time (T_1) of the water protons may be a useful indicator of water mobility, if the ratio of water protons to API protons is sufficiently large, or if the water protons have a correlation time (τ_c) corresponding to the T_1 minimum, such that the T_1 of the water proton is sensitively reflected in the measured T_1 value without being affected by spin diffusion between the water and the API protons. Moreover, even if the ratio of water protons to API protons is not particularly large, and even if water proton does not have a τ_c corresponding to the T_1 minimum, it may be possible to compare the molecular mobility of hydration water in API hydrates based on measured T_1 values, if both of the T_1 of the API proton and the ratio of water protons to API protons are similar for all of the API hydrates compared.

The purpose of this study was to examine the possibility of determining the molecular mobility of hydration water in API hydrates by NMR relaxation measurement. Spin–lattice relaxation, which reflects motions of MHz order, and spin–spin relaxation, which reflects slower motions, were measured for the 11 API hydrates listed in the Japanese Pharmacopeia (JP) using pulsed ^{1}H-NMR, which allows more simplified measurements than high-resolution ^{1}H-NMR. Furthermore, the ease of evaporation of the hydration water was determined under nonisothermal and isothermal conditions using DSC and water vapor sorption isotherm analysis, respectively, and the relationship between the ease of evaporation and the measured values of T_1 and T_2 was examined.

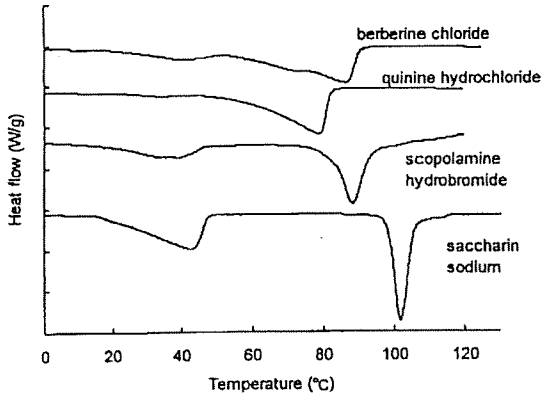

Figure 4. DSC thermograms for API hydrates showing two endothermic peaks.

EXPERIMENTAL

Materials

Cefazolin sodium, ceftazidime, amoxicillin, ampicillin, scopolamine hydrobromide, pipemidic acid, quinidine sulfate hydrates were purchased from Sigma Chemical Co. (St. Louis, MO), and berverine chloride, quinine hydrochloride, saccharin sodium, sulpyrine and di-sodium hydrogen phosphate 12 H_2O were purchased from Wako Pure Chemical Ind. Ltd. (Osaka, Japan), and di-sodium hydrogen phosphate 2 H_2O was from Merck (Darmstadt, Germany).

DOI 10.1002/jps

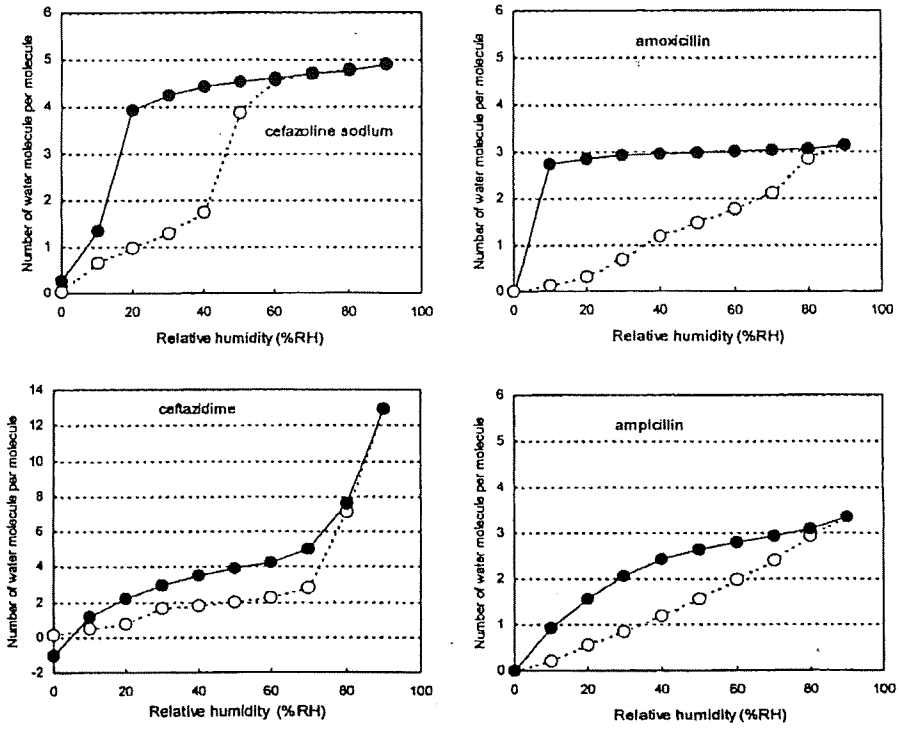

Figure 6. Water sorption isotherms for four antibiotic hydrates.

NMR Relaxation Times

The free induction decay (FID) of protons in API hydrates was obtained using a pulsed NMR spectrometer (25 MHz, JNM-MU25, JEOL, Tokyo, Japan). FID was obtained at 10, 20, 30, and 40°C. The 90° pulses were 2 μs in duration. The "solid echo," with an echo delay of 10 μs, was used in the detection stage of all measurements, in order to overcome the effects of the dead-time.[12] Measurement was repeated four times with a recycling time over five times of the T_1 value measured as described below.

The FID signals obtained between 2.6 and 100 μs that showed only Gaussian-type decay were fitted to Eq. (1) to calculate the T_2 of proton. FID signals obtained for quinidine sulfate and pipemidic acid hydrates showed a small diversion from Gaussian behavior (beat signal) in the final stage of relaxation, suggesting Abragam-type relaxation.[13] However, T_2 was calculated according to Eq. (1) for the purpose of comparison among API hydrates. The FID signals that show both Gaussian and Lorentzian decay patterns were fitted to Eq. (2) representing the summation of the Gaussian and Lorentzian equations.

$$I(t) = I_0 \exp\left[-\left(\frac{t}{T_2}\right)^2\right] \tag{1}$$

$$I(t) = I_0\left[P_G \exp\left(-\left(\frac{t}{T_{2(G)}}\right)^2\right) + P_L \exp\left(-\frac{t}{T_{2(L)}}\right)\right] \tag{2}$$

where $I(t)$ and I_0 are signal intensity at time t and time 0. $T_{2(G)}$ and $T_{2(L)}$ are T_2 for Gaussian decay and Lorentzian decay, respectively, and P_G and P_L are the proportion of protons that show Gaussian decay and Lorentzian decay, respectively.

The T_1 of proton in API hydrates was determined at 30°C by the inversion recovery method. T_1 was calculated according to Eq. (3).

$$I(t) = I_0\left(1 - 2\exp\left(-\frac{t}{T_1}\right)\right) \tag{3}$$

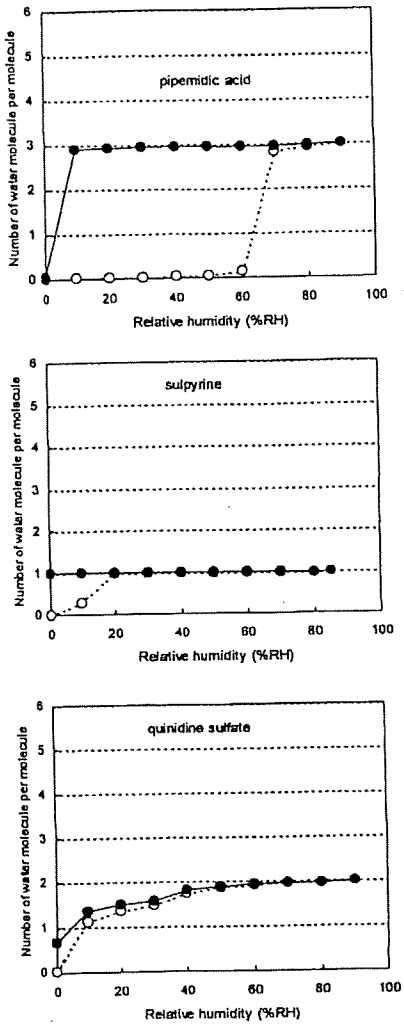

Figure 7. Water sorption isotherms for API hydrates showing a single endothermic peak in DSC thermogram.

Differential Scanning Calorimetry (DSC)

Modulated temperature DSC experiments were performed using a commercial system (2920; TA Instruments, New Castle, DE) attached to a refrigerated cooling accessory. The conditions were as follows: modulation period of 100 s, a modulation amplitude of ±0.5°C, and an underlying heating rate of 1°C/min. Temperature calibration was performed using indium. Samples (approximately 10 mg) were put in a pan without a lid. Nitrogen gas was flowed at 30 mL/min.

Water Sorption Isotherm

Water sorption isotherms were measured gravimetrically at 25°C using the automated sorption analyzer from VTI Corp. (Hialeah, FL). Prior to water sorption and desorption, samples were dried at 60°C and reduced pressure, until the partial vapor pressure became less than 0.0. Equilibrium water content was measured at ascending partial vapor pressures ranging from 0.10 to 0.95, then at descending partial vapor pressures ranging from 0.95 to 0.00 in steps of 0.10 or 0.05. Equilibrium was regarded to have been achieved once the change in sample weight was less than 0.001 mg over 10 min. The limit duration for measurement at a partial vapor pressure was 10 h for scopolamine hydrobromide and 5 h for the others.

RESULTS

NMR Relaxation Times

Figures 1 and 2 show representative examples of the time courses of spin–spin relaxation observed for the 11 API hydrates. Of the four antibiotic hydrates, all exhibited both Gaussian-type decay and Lorentzian decay, as exemplified by ceftazidime and cefazolin sodium hydrates (Fig. 1). The other seven API hydrates exhibited only Gaussian-type decay, as exemplified by quinidine sulfate and scopolamine hydrobromide hydrates (Fig. 2).

In order to calculate the proportion of water protons to API protons, which is required to obtain the T_2 of the water protons by curve-fitting of decay patterns, the number of water molecules per API hydrate molecule was measured by the Karl Fischer method. The results are shown in Table 1, in which the values specified in the JP are also noted for the purpose of comparison. The measured water contents were consistent with those specified in the JP for pipemidic acid, sulpyrine, and quinidine sulfate hydrates, as well as all antibiotic hydrates except for cefazolin sodium hydrate. In contrast, quinine hydrochloride, scopolamine hydrobromide, and saccharin sodium hydrates showed smaller water contents than those specified in the JP.

The time courses of spin–spin relaxation showing both Gaussian decay and Lorentzian decay observed for the four antibiotic hydrates were well fitted to Eq. (2) using the proportion of water protons calculated from the measured water

DOI 10.1002/jps

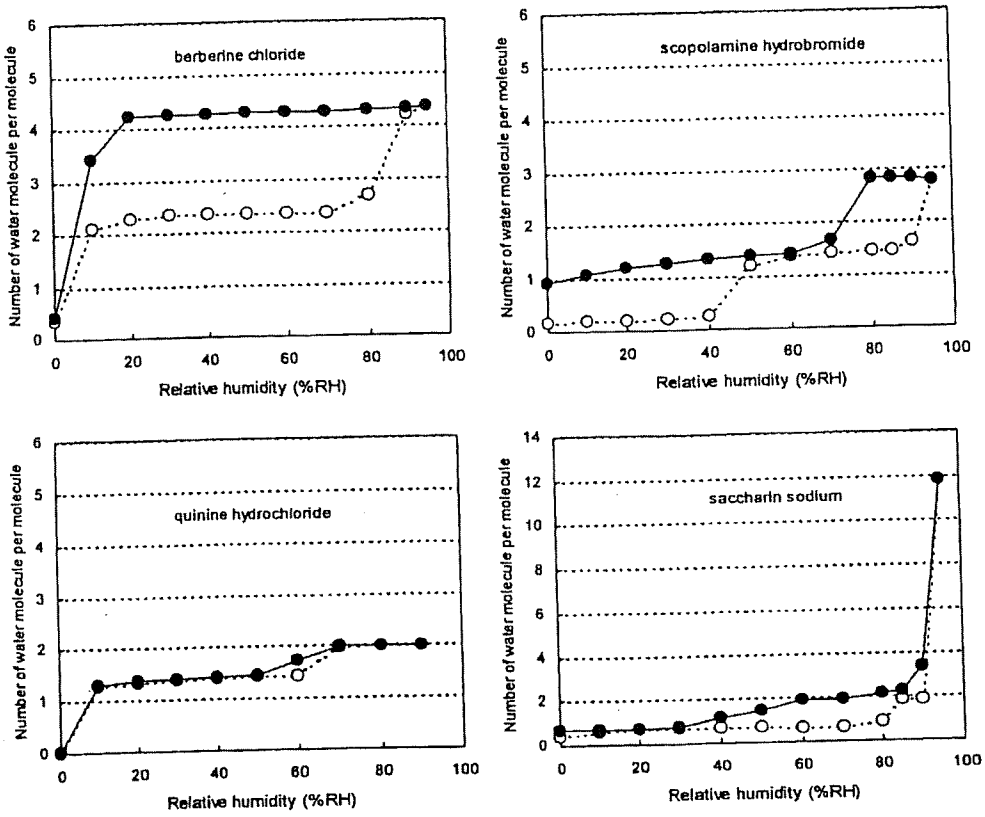

Figure 8. Water sorption isotherms for API hydrates showing two endothermic peaks in DSC thermogram.

content, as shown by the regression curve in Figure 1. Therefore, all of the water protons in the molecule are considered to show Lorentzian decay, and the Gaussian decay is attributed to the drug protons. The T_2 of the Lorentzian decay was calculated according to Eq. (2), and the results will be discussed below. For cefazolin sodium hydrate, better curve-fitting was obtained by regression analysis using a slightly larger value for the proportion of water protons than that calculated from the measured water content. This suggests that a small number of the drug protons exhibit Lorentzian decay; however, it is possible that the water content of the sample used for NMR measurement was different from that of the sample used for Karl Fischer measurements.

The seven API hydrates other than the antibiotic hydrates did not exhibit Lorentzian decay, indicating that all water protons and drug protons in the molecule showed Gaussian decay. The T_2 of the water protons was calculated according to Eq. (1), assuming that the T_2 of the drug protons is similar to that of the water protons. The results will be discussed below.

DSC Thermograms

Figures 3–5 show DSC thermograms measured for the 11 API hydrates. The four antibiotic hydrates, which exhibited Lorentzian decay upon spin–spin relaxation, showed a single endothermic peak due to water evaporation, as shown in Figure 3. In contrast, the API hydrates that did not exhibit Lorentzian decay showed two endothermic peaks (Fig. 4), or one peak (Fig. 5).

The temperature at which an endothermic peak due to water evaporation is observed may be considered to represent the ease of evaporation of hydration water under nonisothermal conditions. The onset temperature was determined as a parameter for approximate comparison of ease of evaporation among the API hydrates, along with ease of evaporation under isothermal conditions as

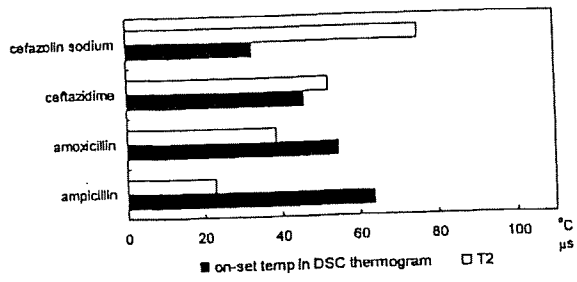

Figure 9. Correlation between onset temperature and T_2 for four antibiotic hydrates.

determined by water vapor sorption analysis. Onset temperature is known to depend on various factors, such as the heating rate, the shapes of the pan and lid, the surface area of the sample, and the flow rate of nitrogen gas. In this study, controllable factors such as the heating rate and the flow rate of nitrogen gas were kept constant, and a pan without a lid was used. The onset temperatures obtained will be discussed below.

Water Vapor Sorption Isotherm

Figures 6–8 show water sorption isotherms observed for the four antibiotic hydrates, the other three API hydrates that exhibited a single endothermic peak due to water evaporation, and the four API hydrates that exhibited two peaks due to water evaporation, respectively. The y-axis represents the number of water molecules per API hydrate molecule, calculated from the water content measured by the Karl Fischer method, assuming that all water molecules present in the sample were evaporated during the drying process (60°C, reduced pressure) prior to the sorption and desorption processes.

The water sorption isotherms (Fig. 6) observed for the four antibiotic hydrates, which exhibited Lorentzian decay upon spin–spin relaxation, indicate that during the desorption process, the water content decreased with decreasing humidity in the range 90–0% RH, with a significant slope in the water content versus humidity plot.

Among the three API hydrates that did not exhibit Lorentzian decay and showed a single endothermic peak due to water evaporation, pipemidic acid and sulpyrine hydrates gave water desorption isotherms in which the water content was constant over a wide humidity range, as shown in Figure 7. Quinidine sulfate also showed a flat line in the water content versus humidity plot, though it was observed only at high humidities.

The water desorption isotherms observed for the other four API hydrates (except berberine chloride), which did not exhibit Lorentzian decay and showed two endothermic peaks due to water evaporation, indicated that the water content remained approximately constant at two levels (Fig. 8).

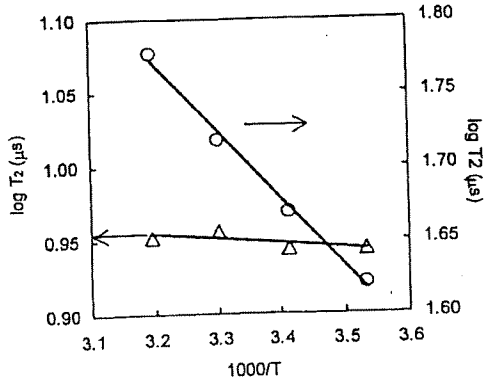

Figure 10. Temperature dependence of T_2 for ceftazidime (circle) and pipemidic acid (triangle) hydrates.

DISCUSSION

The molecular mobility of hydration water in API hydrates was found to vary over a wide range; some, such as ceftazidime hydrate, contain hydration water that shows Lorentzian decay upon spin–spin relaxation, while others contain hydration water that shows Gaussian decay.

Hydration Water Showing Lorentzian Decay

All of the water molecules present in the four antibiotic hydrates were found to exhibit Lorentzian decay, because the proportion of Lorentzian decay was consistent with the proportion of water protons calculated from the water content measured by the Karl Fischer method (Fig. 1). The finding that the water molecules in the antibiotic hydrates showed Lorentzian decay rather than Gaussian decay suggests that water molecules are held in voids in the crystal, rather than being firmly trapped in the crystal lattice. These water molecules may evaporate through channels formed in the interior of the crystal.[14] Hydration water that requires more energy to be released

DOI 10.1002/jps

may exhibit a higher onset temperature of the endothermic peak due to water evaporation in DSC.

The T_2 values determined based on Lorentzian decay is related with τ_c by Eq. (4), such that a smaller value of T_2 represents a larger τ_c (lower mobility).

$$\frac{1}{T_2} = \frac{\gamma^4 \hbar^2 I(I+1)}{5r^6}\left(3\tau_c + \frac{5\tau_c}{1+\omega_0^2\tau_c^2} + \frac{2\tau_c}{1+4\omega_0^2\tau_c^2}\right) \quad (4)$$

where γ, ω_0, I, r, and $\hbar$ are the gyromagnetic ratio, resonance frequency, spin quantum number, spin distance, and the Plank's constant divided by 2π.

As shown in Figure 9, T_2 increased as the onset temperature (Fig. 3) decreased, indicating that hydration water which evaporates at lower temperatures has greater molecular mobility as determined by T_2. This correlation between T_2 and the ease of evaporation under nonisothermal conditions may be explained by assuming that hydration water with a greater T_2 (higher mobility) can escape through channels at a lower temperature.

In order to gain further insight into the correlation between ease of evaporation and the molecular mobility of the hydration water, the ease of evaporation under isothermal conditions was evaluated by water sorption isotherm measurement. Each of the four antibiotic hydrates exhibited a desorption isotherm showing decreases in water content associated with decreases in humidity (Fig. 6). As discussed below, the crystal form of ampicillin hydrate appeared to be altered during the drying process prior to the measurement of water sorption isotherms. Therefore, the isotherm obtained for ampicillin could not be compared with the NMR and DSC data. However, such detrimental effect of predrying was not observed for the other three antibiotic hydrates. The negative water content observed after the desorption process for ceftazidime may be due to chemical degradation occurred under high-humidity conditions or incomplete evaporation of hydration water during predrying. Compared to amoxicillin hydrate, cefazolin sodium hydrate, which has a larger T_2 value, exhibited a greater slope in its water content versus humidity plot. Furthermore, cefazolin sodium exhibited rapid dehydration when humidity was decreased below 20% RH, whereas amoxicillin did not exhibit rapid dehydration until humidity was decreased below 10% RH. These findings suggest that the ease of evaporation of hydration water under isothermal conditions is correlated with molecular mobility as determined by T_2, which supports the conclusion obtained based on DSC measurement. For ampicillin, the slope of the water content versus humidity plot was greater than that of amoxicillin hydrate despite its lower molecular mobility as determined by T_2 and higher onset temperature. This suggests that the drying conditions prior to the sorption and desorption processes were inadequate, which may result in destruction of the crystalline structure. Thus, the isotherm obtained for ampicillin could not be compared with the NMR and DSC data.

As exemplified by ceftazidime hydrate (Fig. 10), T_2 increased significantly with increasing temperature, indicating that T_2 reflects the increases in molecular mobility associated with increases in temperature. Thus, molecular mobility can be considered to correlate with T_2. As shown in Figure 11, antibiotic hydrates with smaller T_2

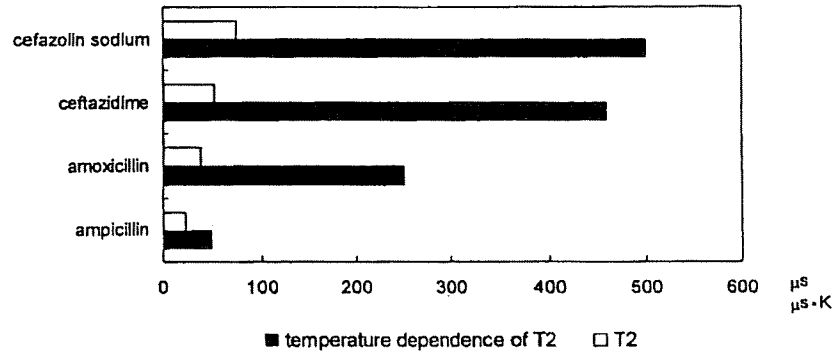

Figure 11. Correlation between T_2 and temperature dependence of T_2 for four antibiotic hydrates.

values showed a smaller change in T_2 with temperature change. This finding suggests that lower values of T_2 reflect a smaller scale of molecular motion, with lower activation energies.

Spin–lattice relaxation time (T_1) is known to reflect molecular mobility, similarly to T_2, but increases with decreasing T_2 (with decreasing molecular mobility) in the slow motional regime. The T_1 values of water protons in the presence of drug protons cannot be determined due to spin diffusion, but an approximate determination of T_1 for water protons is possible if the proportion of water protons is large. For example, in $Na_2HPO_4 \cdot 12H_2O$ and $Na_2HPO_4 \cdot 2H_2O$, water protons are predominant (24/25 and 4/5, respectively). $Na_2HPO_4 \cdot 12H_2O$ exhibits slower spin–spin relaxation (larger T_2) (Fig. 12), and faster spin–lattice relaxation (smaller T_1) (Fig. 13) compared to $Na_2HPO_4 \cdot 2H_2O$, which indicates that both T_1 and T_2 reflect the molecular mobility of hydration water. For the antibiotic hydrates examined, however, correlations between T_1 and T_2 were not observed, as shown in Figure 14. This finding indicates that for API hydrates containing a significant amount of drug protons, such as antibiotic hydrates, the molecular mobility of the hydration water is not reflected in T_1.

Hydration Water Showing Gaussian Decay

As mentioned previously, all of the API hydrates other than the four antibiotic hydrates exhibited only Gaussian decay (Fig. 2). The value of T_2 did not vary significantly among the API hydrates, as shown in Figure 15. Furthermore, the onset temperatures of the single endothermic peaks

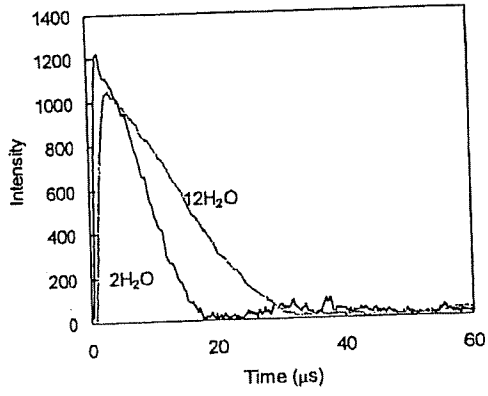

Figure 12. Free induction decay for Na_2HPO_4 $12H_2O$ and $2H_2O$.

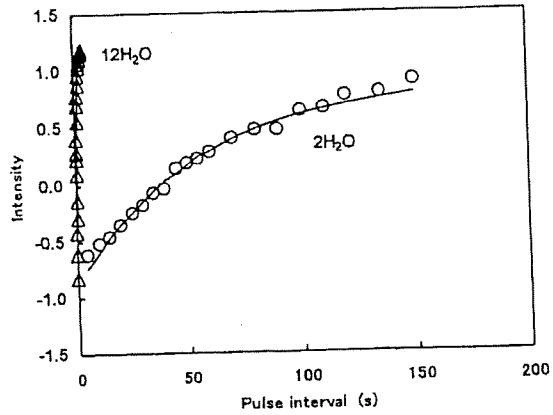

Figure 13. Spin–lattice relaxation for Na_2HPO_4 $12H_2O$ and $2H_2O$.

due to water evaporation for quinidine sulfate, pipemidic acid, and sulpyrine hydrates (Fig. 5), as well as each of the two peaks due to water evaporation observed for quinine hydrochloride, scopolamine hydrobromide, saccharin sodium, and berberine chloride hydrates (Fig. 4), were not correlated with T_2. These findings indicate that the molecular mobility of hydration water that shows Gaussian decay is too low to be reflected in T_2. No correlation between T_2 and molecular mobility is supported by the finding that changes in T_2 associated with changes in temperature were much smaller than those observed for the antibiotic hydrates that exhibited Lorentzian decay, as exemplified by pipemidic acid (Fig. 10). Such low molecular mobility may be attributed to water molecules firmly trapped in the crystal lattice, rather than water molecules trapped in voids in the crystal.

For quinidine sulfate, pipemidic acid, and sulpyrine hydrates, a single endothermic peak was observed in DSC (Fig. 5). The water content versus humidity plots showed a flat line at a certain number of water molecules. Pipemidic acid and sulpyrine showed a flat line at three and one water molecule(s) per hydrate, respectively, and evaporation of these water molecules was observed only under very low humidity (Fig. 7). These findings indicate that water molecules are firmly trapped in the crystal.

For quinine hydrochloride, scopolamine hydrobromide, saccharin sodium, and berberine chloride hydrates, two endothermic peaks were shown in DSC (Fig. 4). The water content versus humidity plots for these hydrates (except for berberine chloride) showed flat lines at two levels

DOI 10.1002/jps

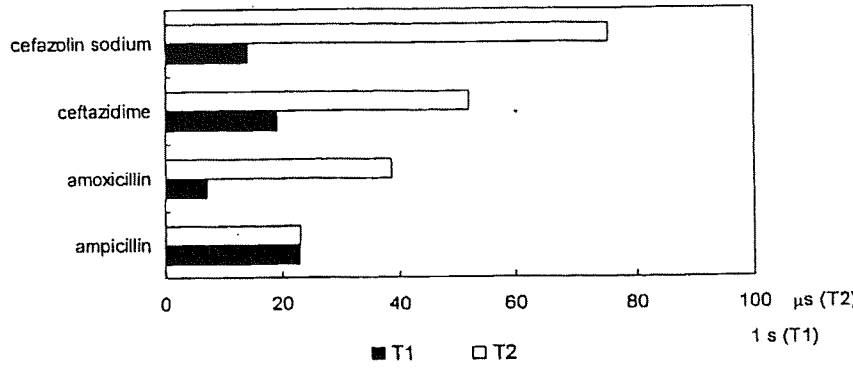

Figure 14. Correlation between T_1 and T_2 for four antibiotic hydrates.

of water content (Fig. 8), suggesting the presence of two water populations: molecules that evaporate at high humidity, and others that evaporate at lower humidity (below 10% RH). This seems to be consistent with the observation of two endothermic peaks in DSC. The endothermic peak observed at a high temperature and the flat line observed at a low humidity may be attributable to hydration water with strong hydrogen–bonding interactions, while the one observed at a lower temperature and higher humidity may be attributable to hydration water with week interactions. The presence of hydration water with week interactions is also supported by the finding that the water contents as measured by the Karl Fischer method were smaller than those specified in the JP (Tab. 1).

CONCLUSION

It was found that spin–spin relaxation time, T_2, is a useful parameter that can indicate the molecular mobility of water of hydration which has relatively high mobility and shows Lorentzian decay upon spin–spin relaxation. For these water molecules, molecular mobility as determined by T_2 is correlated with ease of evaporation both under nonisothermal and isothermal conditions,

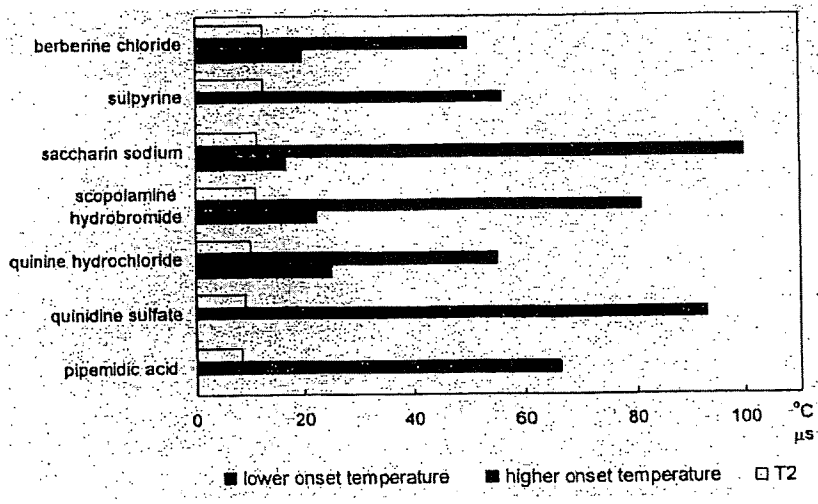

Figure 15. Correlation between onset temperature and T_2 for API hydrates that show Gaussian decay.

such that water molecules with greater ease of evaporation have higher T_2 values.

In contrast, for hydration water that has low mobility and shows Gaussian decay, T_2 was found not to correlate with ease of evaporation under nonisothermal conditions, suggesting that molecular motion that determines the ease of evaporation is not reflected in T_2; in this case, T_2 cannot be used as a parameter to indicate molecular mobility.

The water molecules in the API hydrates studied were found to have wide-ranging molecular mobilities, from low molecular mobility that could not be evaluated by NMR relaxation times, such as the water molecules in pipemidic acid hydrate, to high molecular mobility that could be evaluated by NMR relaxation times, such as the water molecules in ceftazidime hydrate.

REFERENCES

1. Yoshioka S, Aso Y. 2007. Correlations between molecular mobility and chemical stability during storage of amorphous pharmaceuticals. J Pharm Sci 96:960–981.
2. Ahlneck C, Zografi G. 1990. The molecular basis for moisture effects on the physical and chemical stabiity of drugs in the solid state. Int J Pharm 62:87–95.
3. Mimura H, Gato K, Kitamura S, Kitagawa T, Kohda S. 2002. Effect of water content on the solid-state stability in two isomorphic clathrates of cephalosporin: Cefazolin sodium pentahydrte (α form) and KF041 hydrate. Chem Pharm Bull 50: 766–770.
4. Zografi G. 1988. States of water associated with solids. Drug Dev Ind Pharm 14:1905–1926.
5. Newman AW, Reutzel-Edens SM, Zografi G..2007. Characterization of the "hygroscopic" properties of active pharmaceutical ingredients. J Pharm Sci DOI: 10.1002/jps.21033.
6. Brittain HG, Grant DJW. 1999. Effect of polymorphism and solid state solvation on solubility and dissolution rate. In: Brittain HG, editor. Polymorphism in pharmaceutical solids. New York: Marcel Dekker. pp 279–330.
7. Shinyashiki N, Asaka N, Mashimo S. 1990. Dielectric study on dynamics of water in polymer matrix using a frequency range 10^6–10^{10} Hz. J Chem Phys 93:760–764.
8. Ahlqvist MU, Taylor LS. 2002. Water dynamics in channel hydrates investigated using H/D exchange. Int J Pharm 241:253–261.
9. Ruan R, Chen PL. 1998. Mobility of water in food and biological systems. In: Water in foods and biological materials, a nuclear magnetic resonance approach. Lancaster, PA: Technomic Publishing Company, Inc. pp 149–228.
10. Oksanen CA, Zografi G. 1993. Molecular mobility in mixtures of absorbed water and solid poly(vinylpyrrolidone). Pharm Res 10:791–799.
11. Otsuka T, Yoshioka S, Aso Y, Kojima S. 1995. Water mobility in aqueous solutions of macromolecular pharmaceutical excipients measured by oxygen-17 nuclear magnetic resonance. Chem Pharm Bull 43:1221–1223.
12. Mansfield P. 1965. Multiple-pulse nuclear magnetic resonance transients in solids. Phys Rev 137:A961–A974.
13. Parizel N, Meyer G, Weill G. 1993. Nuclear magnetic resonance linesahape studies of interpenetrating polymer networks. Polymer 12:2495–2502.
14. Morris KR. 1999. Structural aspects of hydrates and solvates. In: Brittain HG, editor. Polymorphism in pharmaceutical solids. New York: Marcel Dekker. pp 125–181.

DOI 10.1002/jps

Glass-State Amorphous Salt Solids Formed by Freeze-Drying of Amines and Hydroxy Carboxylic Acids: Effect of Hydrogen-Bonding and Electrostatic Interactions

Saori KADOYA,[a] Ken-ichi IZUTSU,*[,b] Etsuo YONEMOCHI,[a] Katsuhide TERADA,[a] Chikako YOMOTA,[b] and Toru KAWANISHI[b]

[a] *Faculty of Pharmaceutical Sciences, Toho University; 2–2–1 Miyama, Funabashi, Chiba 274–8510, Japan: and* [b] *National Institute of Health Sciences; 1–18–1 Kamiyoga, Setagaya, Tokyo 158–8501, Japan.*
Received February 6, 2008; accepted April 4, 2008; published online April 7, 2008

We studied effect of molecular interactions on the physical properties of binary freeze-dried solids and frozen aqueous solutions using model chemicals containing various functional groups (amino, carboxyl, hydroxyl). Thermal analysis of frozen solutions containing alkyl diamines and hydroxy di- or tricarboxylic acids showed thermal transitions (T_g': glass transition of maximally freeze-concentrated phase) at temperatures higher than those of the individual solutes. A binary frozen solution containing 80 mM 1,3-diamino-2-hydroxypropane (single-solute $T_g' < -60$ °C) and 120 mM citric acid (single-solute T_g': −55.0 °C) made the transition at −30.8 °C. The molecular weight of the solutes had smaller effects on the transition temperatures of the frozen mixture component solutions. Lyophilization of some high T_g' mixture frozen solutions (*e.g.*, 1,3-diamino-2-hydroxypropane and citric acid) resulted in cake-structure amorphous solids with glass transition temperatures (T_g) higher than those of the individual components. Networking of intense hydrogen-bondings and electrostatic interactions between the heterogeneous molecules through the multiple functional groups was suggested to reduce the component mobility in the amorphous freeze-concentrated phase and the freeze-dried solids. Controlling the interactions should be a key to optimizing the physical properties of multi-component amorphous freeze-dried pharmaceutical formulations.

Key words freeze-drying; glass solid; thermal analysis; molecular interaction; salt

Glass-state amorphous solids are applied to pharmaceutical formulations as a way to improve dissolution of hydrophobic active ingredients (APIs) or to ensure stability of embedded biomacromolecules (*e.g.*, recombinant proteins) and drug delivery system (DDS) carriers (*e.g.*, liposome).[1—3] Freeze-drying is often a preferable method over other procedures (*e.g.*, quench-cooling of heat-melt solids) for the large-scale production of glass-state solid formulations containing thermally unstable ingredients. Dispersion of drug molecules into nonionic excipient matrices (*e.g.*, trehalose, polyvinylpyrrolidone (PVP)) is a popular way to make the non-crystalline formulations of many APIs that have intrinsic propensity for crystallization or low glass transition temperatures (T_g).[1] Insufficient miscibility with certain drug molecules and poor storage stability, however, often hinders the development of solid dispersion formulations using the nonionic matrices.

The application of salts or binary complexes is another approach to obtain stable amorphous solids.[4] For example, freeze-drying of sodium indomethacin results in an amorphous solid that has a glass transition temperature (120 °C) significantly higher than that of the free acid molecules (45 °C).[4,5] Recent studies indicated that the glass-state solids composed of excipient salts or salt-forming excipient combinations are promising as dispersion matrices.[6,7] Some pH-adjusting buffer salts (*e.g.*, monosodium citrate) form high T_g amorphous solids applicable to protein formulations.[7] Co-lyophilization of some basic amino acids (*e.g.*, L-arginine, L-lysine, L-histidine) with multivalent inorganic acids (*e.g.*, phosphoric acid) also results in the formation of protein-stabilizing glass-state solids.[6] High transition temperatures of the mixture freeze-dried solids suggest the contribution of strong intermolecular or inter-ion interactions to reducing the heterogeneous component mobility.

In contrast to the extensive studies on the physical properties and local structure of amorphous glass- or rubber-state solids composed of nonionic small molecules (*e.g.*, sucrose, sorbitol) or polymers (*e.g.*, PVP),[3] mechanisms that determine character of organic salts and/or heterogeneous components have not been well elucidated.[1,3] Recent intensive studies on ionic liquids (RTMS: room temperature molten salts) provided valuable information regarding the component ion structures, participating interactions, and the physical properties of the microscopically unordered non-crystalline salt systems.[8] Some earlier studies indicated feasibility to control the physical property of the amorphous salt solids by optimizing the component structure (*e.g.*, ion radius in indomethacin alkali metal salts)[4] and their compositions that determine the intermolecular and/or inter-ion interactions.

The purpose of this study was to elucidate the contribution of functional groups and the size of consisting molecules to the physical properties of multi-component frozen aqueous solutions and their freeze-dried solids. Thermal analysis of various combinations of model chemicals containing amino, carboxyl, and/or hydroxyl groups was performed to obtain the thermal transition temperatures (T_g, T_g': glass transition temperature of maximally freeze-concentrated phase) and propensity for crystallization in the frozen solutions and freeze-dried solids. Mid- and near-infrared analysis was performed to elucidate the molecular interaction in the freeze-dried solids. We also discuss the application of the amorphous mixture solids to pharmaceutical formulations.

* To whom correspondence should be addressed. e-mail: izutsu@nihs.go.jp

Experimental

Materials 1,3-Diaminopropane was purchased from Kanto Kagaku Kogyo Co. (Tokyo, Japan). 1,3-Diamino-2-hydroxypropane was the product of Sigma-Aldrich Inc. (St. Louis, MO, U.S.A.). Tricarballylic acid was obtained from Alfa Aesar GmbH & Co. KG (Karlsruhe, Germany). DL-Malic acid, D-(+)-malic acid, glycolic acid, L-(+)-tartaric acid, glutaric acid, adipic acid, DL-lactic acid (2-hydroxypropanoic acid), 1-aminopropane (propylamine), 1,4-diaminobutane, 1,6-diaminohexane, 1,8-diaminooctane, and other reagents were of analytical grade obtained from Wako Pure Chemical Industries Co. (Osaka, Japan).

Thermal Analysis Thermal analysis of frozen solutions and freeze-dried solids was conducted with a differential scanning calorimeter (DSC Q-10, TA Instruments, New Castle, DE, U.S.A.) with Universal Analysis 2000 software (TA Instruments). An aliquot (10 μl) of aqueous solution in an aluminum cell was cooled to −70 °C at 10 °C/min and then scanned at 5 °C/min. Freeze-dried solids (1—2 mg) in hermetic aluminum cells were scanned from −30 °C at 5 °C/min under nitrogen flow. Physical mixtures containing 1,3-diamino-2-hydroxypropane and citric acid (1.5—2.5 mg) in aluminum cells were melted at 165 °C for 3 min and then cooled rapidly by immersion in liquid nitrogen to prepare quench-cooled melt solids. The cells were transferred to the furnace of the calorimeter at 15 °C and then scanned from −50 °C at 5 °C/min to obtain the glass transition temperatures. Glass transition temperatures were determined as the maximum inflection point of the discontinuities in the heat flow curves.

Freeze-Drying A freeze-drier (Freezone-6, Labconco, Kansas City, MO, U.S.A.) equipped with temperature-controlling trays was used for lyophilization. Aqueous solutions containing the solutes (total 200 mM, 300 μl) in flat-bottom glass vials (13 mm diameter) were placed on the shelf of the freeze-drier at room temperature. The shelf was cooled to −40 °C at 0.5 °C/min and then maintained at that temperature for 2 h before drying. The frozen solutions were dried under vacuum (21 mTorr) maintaining the shelf temperature at −40 °C for 15 h, −30 °C for 6 h, and 35 °C for 6 h. The shelf was heated at 0.2 °C/min between the drying steps. The vials were closed with rubber stoppers under the vacuum. Solids for near-infrared analysis were prepared by freeze-drying the aqueous solutions (1 ml) in larger vials (18 mm diameter).

Mid- and Near-Infrared Spectroscopy (IR, NIR) An FT-IR spectrophotometer (MB104, ABB Bomen, Quebec, Canada) and GRAMS/32 software (Galactic Ind. Co., Salem, NH, U.S.A.) were used to obtain mid-infrared spectra of the solids (approx. 1 mg sample solid) in a pressed potassium bromide disk (approx. 250 mg). Transition spectra of the sample disks were obtained at 4 cm^{-1} resolution in 128 scans. Near-infrared spectroscopy was performed by using a Bruker MPA system with a diffuse-reflectance integrating-sphere probe (PbS detector) and OPUS software (Ettlingen, Germany). Near-infrared light was directed upward from the bottom of the glass vials containing freeze-dried solids to obtain the reflected signal over a range of 4000—12000 cm^{-1} with a resolution of 4 cm^{-1} in 128 scans.

Powder X-Ray Diffraction (XRD) and Residual Water Content Measurement The powder X-ray diffraction patterns were measured at room temperature with a Rint-Altima diffractometer (Rigaku, Tokyo, Japan) with Cu$K\alpha$ radiation at 40 kV/40 mA. The samples were scanned in the area of $5° < 2\theta < 35°$ at an angle speed of 5°/min. An AQV-6 volumetric titrator (Hiranuma Sangyo, Ibaraki, Japan) was used to determine the amount of water in the freeze-dried solids suspended in dehydrated methanol by the Karl–Fischer method.

Results

Figure 1 shows thermograms of frozen aqueous solutions containing a carboxylic acid and an amide (200 mM). The structure of the chemicals used in this study and their physical properties in the frozen solutions obtained by thermal analysis are summarized in Table 1. Some solutes showed intrinsic propensities to crystallize in the freeze-concentrated phases. An endotherm (−15.8 °C) in a frozen malonic acid solution suggested melting of the eutectic crystal. The exotherm (−53.1 °C) and endotherm (−19.3 °C) peaks

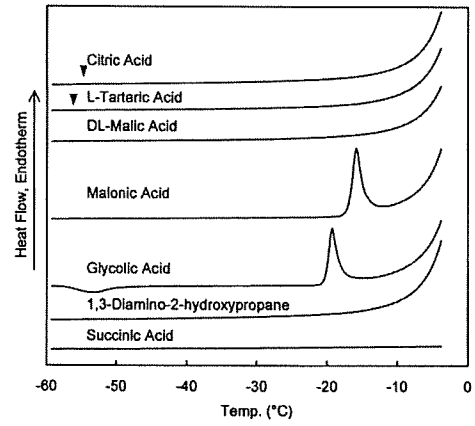

Fig. 1. Thermograms of Frozen Solutions Containing a Carboxylic Acid or an Amine (200 mM)

Aliquots (10 μl) of solutions in hermetic aluminum cells were scanned from −70 °C at 5 °C/min. Arrowheads denote the glass transition of maximally freeze-concentrated solutes (T_g').

Table 1. Structure and Thermal Property of Carboxylic Acids and Amines in Frozen Aqueous Solutions Obtained by Thermal Analysis

	MW	Functional groups			Property in frozen solutions	
		COOH	OH	NH_2	Crystallinity	Thermogram
Acetic acid	60.1	1	0	0	Crystallized	Endotherm
Glycolic acid	76.1	1	1	0	Crystallized	Exotherm/endotherm
DL-Lactic acid	90.1	1	1	0	Amorphous	T_g' <−60 °C
Malonic acid	104.1	2	0	0	Crystallized	Endotherm
Succinic acid	118.1	2	0	0	Crystallized	Flat
Glutaric acid	132.1	2	0	0	Crystallized	Flat
Adipic acid	146.1	2	0	0	Crystallized	Exotherm
Pimeric acid	160.2	2	0	0	Crystallized	Flat
L-Malic acid	134.1	2	1	0	Amorphous	T_g' <−60 °C
L-Tartaric acid	150.1	2	2	0	Amorphous	T_g': −57.1 °C
Tricarballylic acid	176.1	3	0	0	Amorphous	T_g': −52.1 °C
Citric acid	192.1	3	1	0	Amorphous	T_g': −55.1 °C
1-Aminopropane	59.1	0	0	1	Crystallized	Endotherm
3-Amino-1-propanol	75.1	0	1	1	Amorphous	T_g' <−60 °C
1,3-Diaminopropane	74.1	0	0	2	Amorphous	T_g' <−60 °C
1,4-Diaminobutane	88.2	0	0	2	Crystallized	Endotherm
1,6-Diaminohexane	116.2	0	0	2	Crystallized	Endotherm
1,8-Diaminooctane	144.3	0	0	2	Crystallized	Flat
1,3-Diamino-2-hydroxypropane	90.1	0	1	2	Amorphous	T_g' <−60 °C

observed in a heating scan of a frozen glycolic acid solution indicated eutectic crystallization and subsequent melting, respectively. The flat thermogram of a frozen succinic acid solution up to the ice-melting temperature suggested crystallized solutes. Some of these frozen solutions showed an exotherm that indicated eutectic crystallization in the cooling process before the thermal scan (data not shown). L-Tartaric acid and citric acid remained amorphous in the freeze-concentrated phase, presenting glass transition of the maximally freeze-concentrated solute phase (T_g') at $-55.1\,°C$ and $-57.1\,°C$, respectively.[7] The absence of particular thermal transitions and the gradual shift of the thermogram in some other single-solute frozen solutions (*e.g.*, DL-malic acid, 1,3-diamino-2-hydroxypropane) suggested that T_g' transition of the amorphous concentrated phase occurred at temperatures below the measurement temperature range ($<-60\,°C$).

Figures 2 and 3 show T_g' of frozen binary solutions containing various diamines and L-tartaric acid or citric acid. Most of the solute combinations showed a bell-shaped profile of T_g' that depended largely on the number of functional groups in the amines. Frozen mixture solutions containing amines and citric acid showed the T_g' peaks at lower acid molar ratios than in the combination with L-tartaric acid. Transition temperatures (T_g') of frozen solutions containing the acids and various diamines were significantly higher than those of the mixtures with monoamines (*e.g.*, 1-aminopropane). Slightly higher transition temperatures of the frozen solutions containing citric acid and 1,8-diaminooctane compared to those with smaller alkyldiamines (*e.g.*, 1,3-diaminopropane) indicated a relatively small effect of the component molecular size on the T_g' of the mixture phases. Introduction of hydroxyl groups to a diamine (*e.g.*, 1,3-diaminopropane to 1,3-diamino-2-hydroxypropane) raised the T_g' of the frozen mixture solutions to some extent. Mixing with L-tartaric acid or citric acid prevented crystallization of some amines (*e.g.*, 1,4-diaminobutane) in the frozen solutions. In contrast, some frozen mixture solutions showed thermal peaks that suggested crystallization of the salts. For example, a frozen solution containing 60 mM diaminooctane and 140 mM L-tartaric acid showed a T_g' ($-32.7\,°C$) and a eutectic crystallization exotherm peak ($-19.9\,°C$) in a thermal scan (data not shown).

Mixing of 1,3-diamino-2-hydroxypropane and some carboxylic acids (*e.g.*, succinic acid) also induced a significant upward shift of the T_g' (Fig. 4). The transition temperatures depended largely on the compositions of the carboxyl and hydroxyl groups in the acids. Most of the frozen mixture solutions showed the highest T_g' at the solute concentration ratios relatively rich in carboxylic acid. Alkyl chain length of the dicarboxylic acids gave limited effects on the T_g' of the mixture frozen solutions. DL-Malic acid and D-malic acid presented virtually identical T_g' profiles of the mixture frozen solutions. Mixing with 1,3-diamino-2-hydroxypropane prevented crystallization of some dicarboxylic acids (*e.g.*, malonic acid, pimeric acid) in the frozen solutions (data not shown). High T_g' of the frozen solutions containing 1,3-diamino-2-hydroxypropane and the hydroxy carboxylic acids (DL-malic acid, L-tartaric acid, citric acid) indicated a large effect of the hydroxyl group in reducing the component mobility in the freeze-concentrated phase. Frozen solutions containing 1,3-diamino-2-hydroxypropane and acetic acid or

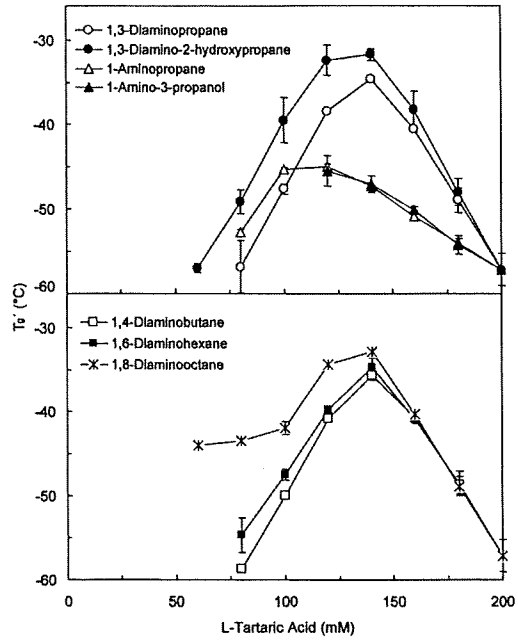

Fig. 2. Glass Transition Temperatures of the Maximally Freeze-Concentrated Phase (T_g') of Frozen Aqueous Solutions Containing L-Tartaric Acid and Various Amines

Frozen solutions (10 μl, 200 mM total) were scanned from −70 °C at 5 °C/min (n=3).

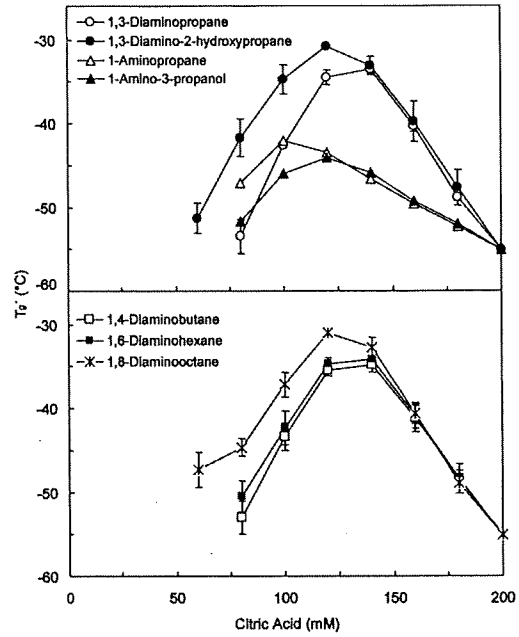

Fig. 3. Glass Transition Temperatures of the Maximally Freeze-Concentrated Phase (T_g') of Frozen Aqueous Solutions Containing Citric Acid and Various Amines

Frozen solutions (10 μl, 200 mM total) were scanned from −70 °C at 5 °C/min (average±S.D., n=3).

glycolic acid showed a gradual shift of the thermograms that suggested an amorphous mixture freeze-concentrated phase with T_g' below the measurement temperature range ($<-60\,°C$) (data not shown). The absence of apparent thermal transitions in frozen solutions containing some dicarboxylic

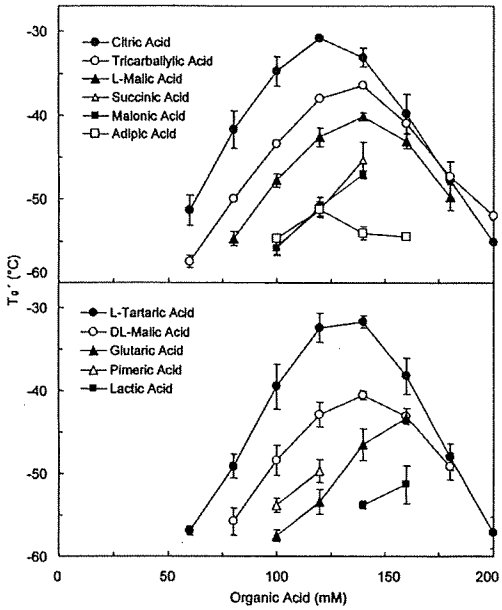

Fig. 4. Glass Transition Temperatures of the Maximally Freeze-Concentrated Phase (T_g') of Frozen Aqueous Solutions Containing 1,3-Diamino-2-hydroxypropane and Various Carboxylic Acids

Frozen solutions (10 μl, 200 mM total) were scanned from −70 °C at 5 °C/min (average±S.D., n=3).

acids (*e.g.*, succinic acid) and diamines (*e.g.*, diaminopropane) also suggested a large contribution of the hydroxyl groups to forming the high T_g' freeze-concentrated phase (data not shown).

Aqueous solutions containing 1,3-diamino-2-hydroxypropane and a hydroxy carboxylic acid (*e.g.*, DL-malic acid, L-tartaric acid, citric acid, 200 mM total) were freeze-dried to examine the physical properties of the resulting solids. The primary drying process at a shelf temperature (−40 °C) induced physical collapse in some lower T_g' (<−40 °C) samples, presumably because of the large molecular mobility of the freeze-concentrated phase.[9] Other frozen solutions were freeze-dried as cake-structure solids. Thermal analysis of the freeze-dried cake-structure mixture solids showed glass transitions (T_g) as high as 60.2 °C (Fig. 5, 120 mM 1,3-diamino-2-hydroxypropane, 80 mM citric acid). The solids freeze-dried from solutions containing 1,3-diamino-2-hydroxypropane and citric acid or L-tartaric acid at a 1 : 1 molar ratio showed amorphous components (halo patterns in the powder X-ray diffraction analysis) that have relatively high residual water (approx. 7—9%, w/w, data not shown). Amorphous solids of pure citric acid and 1,3-diamino-2-hydroxypropane were not available in the freeze-drying because of the physical collapse and crystallization that occurred during the process.

Quench-cooled heat-melt mixture solids containing 1,3-diamino-2-hydroxypropane and citric acid also showed a mixing-induced upward shift of the glass transition temperatures (Fig. 6). The highest transition temperature (54.5 °C) of the 0.4 citric acid molar fraction was slightly lower than that of the freeze-dried solid. Citric acid showed the glass transition of the quench-cooled solid at 9.5 °C.[10—12] The T_g of amorphous 1,3-diamino-2-hydroxypropane was not available using this method, and its low melting temperature (approx. 40—44 °C) strongly suggested a T_g below 0 °C (data not shown).

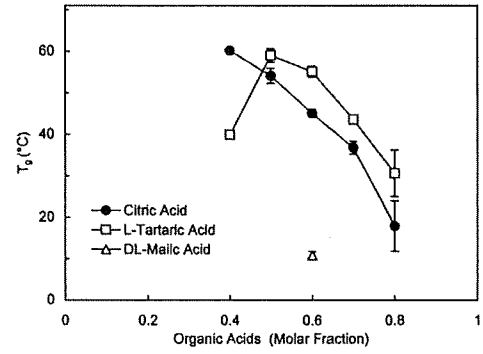

Fig. 5. Glass Transition Temperatures (T_g) of Freeze-Dried Solids Containing 1,3-Diamino-2-hydroxypropane and Organic Acids

The solids (1—2 mg) obtained by freeze-drying of aqueous solutions (200 mM total) were scanned from −30 °C at 5 °C/min (average±S.D., n=3).

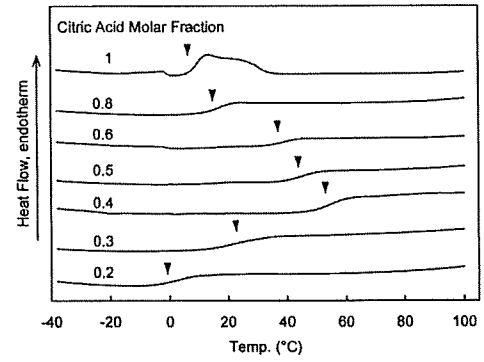

Fig. 6. Thermograms of Quench-Cooled Melt Mixture Solids Containing 1,3-Diamino-2-hydroxypropane and Citric Acid

The solids (1.5—2.5 mg) obtained by immersion of the heat-melt into liquid nitrogen were scanned from −30 °C at 5 °C/min.

Mid-infrared analysis (FT-IR, KBr tablet transmission) of the amorphous mixture solids (0.5 citric acid molar fraction) prepared by freeze-drying and quench-cooling showed broad absorption bands (Fig. 7). Some relatively weak bands (*e.g.*, 1568 cm^{-1}) in the quench-cooled solid suggested evaporation of 1,3-diamino-2-hydroxypropane in the heating process. Non-destructive diffuse-reflection near-infrared (NIR) analysis of the freeze-dried mixture solids also showed broad bands typical for the amorphous solids (Fig. 8). Absence of some bands (*e.g.* N–H stretch 1st overtone of amino group at 6519 cm^{-1})[13] in the co-lyophilized solid (0.5 citric acid molar fraction) strongly suggested the interaction between the heterogeneous components that altered environment around the functional groups.

Discussion

Mixing of the alkyl diamines and hydroxy di- or tri-carboxylic acids induced high transition temperature amorphous concentrated phases in frozen aqueous solutions.[14] Some of the solute combinations formed cake-structure glass-state amorphous solids during freeze-drying. The high transition temperatures (T_g' and T_g) should allow faster drying processes at higher product temperature without physical collapse or shrinking of the solids.[9,15—17] Primary drying should

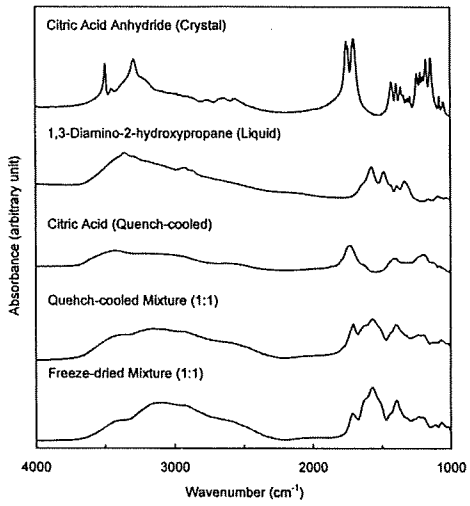

Fig. 7. FT-IR Spectra of Solids Containing 1,3-Diamino-2-hydroxypropane and Citric Acid

The mixture solids were obtained by quench-cooling of a melt (1 : 1 molar ratio, 165 °C, 3 min) or by freeze-drying of a solution (100 mM each).

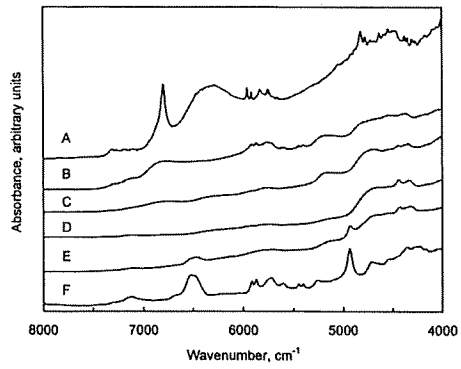

Fig. 8. Diffuse-Reflection Near-Infrared Spectra of Samples Containing 1,3-Diamino-2-hydroxypropane and Citric Acid

Each line denotes spectrum of anhydrous citric acid crystal powder (A), quench-cooled anhydrous citric acid melt (B), 1,3-diamino-2-hydroxypropane liquid (F), and solid lyophilized at the citric acid molar fraction of 0.3 (C), 0.5 (D), 0.7(E).

be conducted below the collapse temperature of the system (T_c), usually adjacent to and/or several degrees higher than the T_g', to obtain the pharmaceutically acceptable cake-structure solids. The primary drying is usually conducted at above −40 °C to accomplish ice sublimation on a practical timescale. Exposure of the partially dried solids above their glass transition temperature in the secondary drying process may shrink the cakes.

The bell-shaped profiles of the transition temperatures (T_g', T_g) depending on the component concentration ratio suggested strong attractive interaction between the components in the amorphous freeze-concentrated phase and the freeze-dried solids. Ideal mixing of nonionic molecules without particular attractive or repulsive interactions resulted in their glass transition at temperatures between those of the individual components, following the Gordon–Taylor equation.[11,18–20] It is also empirically known that frozen solutions containing the nonionic solute combinations have their thermal transition at temperatures (T_g') between those of individual solutes.[21,22] Significant upward deviation of the transition temperatures from those in the equation indicated the strong attractive interaction between the heterogeneous components. The mixing-induced transition temperature shift is also described as increasing "effective molecular weights" because many nonionic molecules (*e.g.*, polyols, saccharides) have the thermal transitions of the amorphous solids (T_g) or frozen solutions (T_g') at higher temperatures upon increasing the molecular weights.[23,24]

Networking of intense electrostatic interactions and hydrogen-bondings between the multiple functional groups should be a primary mechanism that raises the transition temperatures of the freeze-concentrated solute mixture phase and the freeze-dried solids.[4,6,25] The alkyl diamines and hydroxy di- or tri-carboxylic acids form ion pairs in aqueous solutions, and possibly in the freeze-concentrated phase. Some protonated polyamines selectively and strongly interact with particular dicarboxylates in aqueous solutions.[26] The ammonium carbohydrate ion pairs form multiple hydrogen-bonding in some non-polar solvents.[27,28] Continuous network of electrostatic interactions and hydrogen-bonding make the salt crystals popular supermolecular building blocks.[29] The differently protonated carboxyl and carboxylate groups also form an intermolecular hydrogen-bonding anion network.[30] It is plausible that the multi-component interactions contribute to the high transition temperature of the amorphous freeze-concentrated phase (T_g') and the freeze-dried solids (T_g). The eutectic crystallization observed in some high T_g' frozen solutions (*e.g.*, 60 mM diaminooctane and 140 mM L-tartaric acid) suggested effective interactions that induce the spatial ordering of the salt components above the transition temperature. Introduction of the hydroxyl groups to the components should provide additional hydrogen bonding in the amorphous phases. The limited effect of the component size on the transition temperatures also supported the significance of the interaction networks in determining physical properties.[23] Various factors, including the component structures, molar ratios, and water contents should alter the contribution of hydrogen-bonding and electrostatic (*e.g.*, ion–ion, ion–dipole, dipole–dipole) interactions in the amorphous phases. Further information on the interactions remains to be elucidated by other analytical methods (*e.g.*, solid-state NMR).

Recent studies on ionic liquids (RTMS: room temperature molten salt) also indicated the significant contribution of intermolecular (inter-ion) interactions to determining the physical properties of the locally disordered liquid or amorphous solid systems.[31,32] Factors that provide weak interaction between the molecules and/or ions (*e.g.*, size, charge distribution, functional groups) should induce low glass transition temperatures and low viscosities relevant to ionic liquids.[8] In contrast, glass-state solids would be designed by introducing strong interactions between the heterogeneous components.

The glass-state multi-component amorphous solids should be applicable in pharmaceutical formulations in several ways. Certain excipient mixture glass solids would become molecular dispersion matrixes that enable rapid dissolution of active ingredients or stabilization of biomacromolecules.[6] Some basic amino acids (*e.g.*, L-arginine) would be practical choices to form the glass-state mixture solids applicable in pharmaceutical formulations. The weakly acidic to alkaline pH of the high T_g mixtures and their re-hydrated solutions

would be preferable to ensure the storage stability of embedded molecules, as well as to reduce local stimulation in the site of parenteral application. Some pharmaceutically active ingredients (APIs) that have multiple amino or carboxyl groups may also form glass-state solids by direct interactions in mixing with some excipients.

References

1) Hancock B. C., Zografi G., *J. Pharm. Sci.*, **86**, 1—12 (1997).
2) Yu L., *Adv. Drug Deliv. Rev.*, **48**, 27—42 (2001).
3) Hilden L. R., Morris K. R., *J. Pharm. Sci.*, **93**, 3—12 (2004).
4) Tong P., Taylor L. S., Zografi G., *Pharm. Res.*, **19**, 649—654 (2002).
5) Tong P., Zografi G., *Pharm. Res.*, **16**, 1186—1192 (1999).
6) Izutsu K., Fujimaki Y., Kuwabara A., Aoyagi N., *Int. J. Pharm.*, **301**, 161—169 (2005).
7) Shalaev E. Y., Johnson-Elton T. D., Chang L., Pikal M. J., *Pharm. Res.*, **19**, 195—201 (2002).
8) Ohno H., *Bull. Chem. Soc. Jpn.*, **79**, 1665—1680 (2006).
9) Nail S. L., Jiang S., Chongprasert S., Knopp S. A., *Pharm. Biotechnol.*, **14**, 281—360 (2002).
10) Lu Q., Zografi G., *J. Pharm. Sci.*, **86**, 1374—1378 (1997).
11) Summers M. P., *J. Pharm. Sci.*, **67**, 1606—1610 (1978).
12) Timko R. J., Lordi N. G., *J. Pharm. Sci.*, **71**, 1185—1186 (1982).
13) Shenk J. S., Workman J. J., Jr., Westerhaus M. O., "Handbook of Near-Infrared Analysis," ed. by Burns D. A., Ciurczak E. W., Marcel Dekker, New York, 2001, pp. 419—474.
14) Akers M. J., Milton N., Byrn S. R., Nail S. L., *Pharm. Res.*, **12**, 1457—1461 (1995).
15) MacKenzie A. P., *Bull. Parenter. Drug Assoc.*, **20**, 101—130 (1966).
16) Tang X., Pikal M. J., *Pharm. Res.*, **21**, 191—200 (2004).
17) Akers M. J., Vasudevan V., Stickelmeyer M., *Pharm. Biotechnol.*, **14**, 47—127 (2002).
18) Gordon M., Taylor J. S., *J. Appl. Chem.*, **2**, 493—500 (1952).
19) Shamblin S. L., Taylor L. S., Zografi G., *J. Pharm. Sci.*, **87**, 694—701 (1998).
20) Hoppu P., Jouppila K., Rantanen J., Schantz S., Juppo A. M., *J. Pharm. Pharmacol.*, **2007**, 373—381 (2007).
21) Chang B. S., Randall C., *Cryobiology*, **29**, 632—656 (1992).
22) "Heat and Mass Transfer Issues in Freeze-Drying Process Development," ed. by Rambhatla S., Pikal M. J., American Association of Pharmaceutical Scientists, Arlington, 2004, pp. 75—109.
23) Levine H., Slade L., *J. Chem. Soc., Faraday Trans. 1*, **84**, 2619—2633 (1988).
24) Franks F., *Dev. Biol. Stand.*, **74**, 9—18 (1992).
25) Mattern M., Winter G., Kohnert U., Lee G., *Pharm. Dev. Technol.*, **4**, 199—208 (1999).
26) Hosseini M. W., Lehn J.-M., *Helv. Chim. Acta*, **69**, 587—603 (1986).
27) Yerger E. A., Barrow G. M., *J. Am. Chem. Soc.*, **77**, 6206—6207 (1955).
28) Sada K., Watanabe T., Miyamoto J., Fukuda T., Tohnai N., Miyata M., Kitayama T., Maehara K., Ute K., *Chem. Lett.*, **33**, 160—161 (2004).
29) Sada K., Tani T., Shinkai S., *Synlett*, **2006**, 2364—2374 (2006).
30) Kobayashi N., Naito T., Inabe T., *Bull. Chem. Soc. Jpn.*, **76**, 1351—1362 (2003).
31) Fukumoto K., Yoshizawa M., Ohno H., *J. Am. Chem. Soc.*, **127**, 2398—2399 (2005).
32) Yamamuro O., Minamimoto Y., Inamura Y., Hayashi S., Hamaguchi H., *Chem. Phys. Lett.*, **423**, 371—375 (2006).

Glycosylation Analysis of IgLON Family Proteins in Rat Brain by Liquid Chromatography and Multiple-Stage Mass Spectrometry†

Satsuki Itoh,‡ Akiko Hachisuka,‡ Nana Kawasaki,*,‡,§ Noritaka Hashii,‡ Reiko Teshima,‡ Takao Hayakawa,∥ Toru Kawanishi,‡ and Teruhide Yamaguchi‡

Division of Biological Chemistry and Biologicals, National Institute of Health Sciences, 1-18-1, Kamiyoga, Setagaya-ku, Tokyo 158-8501, Japan, Core Research for Evolutional Science and Technology of Japan Science and Technology Agency, Kawaguchi Center Building, 4-1-8 Hon-cho, Kawaguchi, Saitama 332-0012, Japan, and Pharmaceutical Research and Technology Institute, Kinki University, 3-4-1 Kowakae, Higashi-Osaka 577-8502, Japan

Received May 23, 2008; Revised Manuscript Received July 17, 2008

ABSTRACT: IgLON family proteins, including limbic-associated membrane protein (LAMP), opioid-binding cell adhesion molecule (OBCAM), neurotrimin, and Kilon, are immunoglobulin (Ig) superfamily cell adhesion molecules. These molecules are composed of three Ig domains and a glycosylphosphatidylinositol (GPI) anchor and contain six or seven potential N-glycosylation sites. Although their glycosylations are supposed to be associated with the development of the central nervous system like other Ig superfamily proteins, they are still unknown because of difficulty in isolating individual proteins with a high degree of homology in performing carbohydrate analysis. In this study, we conducted simultaneous site-specific glycosylation analysis of rat brain IgLON proteins by liquid chromatography and multiple-stage mass spectrometry (LC−MS^n). The rat brain GPI-linked proteins were enriched and separated by sodium dodecyl sulfate−polyacrylamide gel electrophoresis. The four proteins were extracted from the gel, and subjected to LC−MS^n after proteinase digestions. A set of glycopeptide MS data, including the mass spectrum, the mass spectrum in the selected ion monitoring mode, and the product ion spectra, was selected from all data based on carbohydrate-related ions in the MS/MS spectrum. The peptide portion and the carbohydrate structure were identified on the basis of peptide-related ion and carbohydrate-related ions, and the accurate mass. The site-specific glycosylations of four proteins were elucidated as follows. *N*-Glycans near the N-terminal were disialic acid-conjugated complex- and hybrid-type oligosaccharides. The first Ig domains were occupied by Man-5-9. Diverse oligosaccharides, including Lewis a/x-modified glycans, a brain-specific glycan known as BA-2, and Man-5, were found to be attached to the third Ig domain. Three common structures of glycans were found in the GPI moiety of LAMP, OBCAM, and neurotrimin.

Cell adhesion molecules on cell surfaces are involved in several biological events, such as cell−cell interaction, signaling, and cellular traffic. In the central nervous system, cell adhesion molecules are associated with the differentiation and migration of neurons, and neurite outgrowth. The immunoglobulin (Ig) superfamily, which contains one or more Ig-like domains, is known as one of the cell adhesion molecule families in the central nervous system (*1*). The Ig superfamily includes various proteins, such as P0, Thy-1, myelin-associated glycoprotein (MAG), neural cell adhesion molecule (NCAM), L1, contactin, and IgLON family proteins. Glycosylation of the Ig superfamily proteins is known to be involved in cell−cell interactions (*2*−*4*). Polysialylated glycans in the fifth domain of NCAM are thought to inhibit the interaction of NCAM with other molecules and to promote neural plasticity through a repulsive interaction (*5*, *6*). The HNK-1 epitope in the third and fifth domains of NCAM is known to mediate molecular recognition in the nervous system (*7*).

The IgLON superfamily includes the limbic-associated membrane protein (LAMP),[1] the opioid-binding cell adhesion molecule (OBCAM), neurotrimin, and Kilon (*8*−*14*), and

† This work was supported in part by a Grant-in-Aid from the Ministry of Health and Labor and Welfare, and Core Research for Evolutional Science and Technology Program (CREST) of the Japan Science and Technology Agency (JST).

* To whom correspondence should be addressed: Division of Biological Chemistry and Biologicals, National Institute of Health Sciences, 1-18-1, Kamiyoga, Setagaya-ku, Tokyo 158-8501, Japan. Telephone: +81-3-3700-9074. Fax: +81-3-3707-6950. E-mail: nana@nihs.go.jp.

‡ National Institute of Health Sciences.

§ Core Research for Evolutional Science and Technology of Japan Science and Technology Agency.

∥ Kinki University.

[1] Abbreviations: LC, liquid chromatography; MS, mass spectrometry; MS^n, multiple-stage mass spectrometry; LAMP, limbic-associated membrane protein; OBCAM, opioid-binding cell adhesion molecule; GlcNAc, *N*-acetylglucosamine; GPI, glycosylphosphatidylinositol; PI-PLC, phosphatidylinositol-specific phospholipase C; PNGase F, peptide *N*-glycosidase F; IT-MS, ion trap mass spectrometer; FT ICR-MS, Fourier transform ion cyclotron resonance mass spectrometer; GCC, graphitized carbon column; TIC, total ion chromatogram; CID, collision-induced dissociation; SIM, selected ion monitoring; dHex, deoxyhexose; Hex, hexose; HexNAc, *N*-acetylhexosamine; Fuc, fucose; Man, mannose; Gal, galactose; GlcNAc, *N*-acetylglucosamine; GlcN, glucosamine; NeuAc, *N*-acetylneuraminic acid; $EtNH_2$, ethanolamine; Ino, inositol; BA-2, brain-specific sugar chain, GlcNAcβ1−2Manα1−6(GlcNAcβ1−4)(GlcNAcβ1−2Manα1−3)Manβ1−4GlcNAcβ1−4(Fucα1−6)GlcNAc; SDS−PAGE, sodium dodecyl sulfate−polyacrylamide gel electrophoresis.

10.1021/bi8009778 CCC: $40.75
Published on Web 08/26/2008